Chinese Chemical Letters 32 (2021) 1348–1358

Contents lists available at ScienceDirect

Chinese Chemical Letters

journal homepage: www.elsevier.com/locate/cclet

Review

Photo-responsive metal/semiconductor hybrid nanostructure: A promising electrocatalyst for solar light enhanced fuel cell reaction

Jiayue Hu[a], Chunyang Zhai[b], Mingshan Zhu[a,*]

[a] Guangdong Key Laboratory of Environmental Pollution and Health, School of Environment, Jinan University, Guangzhou 511443, China
[b] School of Materials Science and Chemical Engineering, Ningbo University, Ningbo 315211, China

ARTICLE INFO

Article history:
Received 3 September 2020
Received in revised form 21 September 2020
Accepted 27 September 2020
Available online 28 September 2020

Keywords:
Direct alcohol fuel cells
Semiconductor materials
Noble metal
Photo-responsive electrocatalysis
Hybrid material

ABSTRACT

Direct alcohol fuel cells (DAFCs) have received wide attention as a new type of clean energy device because of their high energy conversion efficiency, portability, non-toxicity and pollution-free. Anode catalysts are the key factors affecting the performance of DAFCs. Recently studies show that using the optical activity of semiconductor materials as the carriers of traditional precious metal electrocatalysts, under the illumination of light sources, can greatly improve the electrocatalytic activity and stability of electrodes. In this review, the research progress of photo-responsive metal/semiconductor hybrids as the electrocatalysts for DAFCs in recent years is summarized, including: (1) Mechanism and advantages of photo-assistant electrochemical alcohol oxidation reaction, (2) metal/semiconductor electrocatalyst for the different type of fuel cell reactions, (3) different kind of metals in photo-responsive metal/semiconductor hybrid nanostructure, (4) the personal prospects of the photo-responsive metal/semiconductor electrode for future application in DAFCs.

1. Introduction

In recent years, with the depletion of fossil fuels and the increasing environmental pollution, special attention is being paid for clean and renewable energy sources [1–8]. As new energy-efficient conversion energy and pollution-free sources, direct alcohol fuel cells (DAFCs) have attracted wide attention. DAFC is an electronic device that directly converts the chemical energy of small organic molecules such as methanol, ethanol, formic acid and ethylene glycol into electrical energy, and has high conversion efficiency [1–4,9–11].

However, the large-scale application of DAFCs is still overcome by many technical difficulties. Among them, anode catalysts as the core components of DAFCs are also the focus of research in recent years. Researching high performance, low cost anode catalysts are the main technical barriers affecting commercial applications of DAFCs. The catalysts usually used today are composed of a precious metal and a carrier [5–7]. As we all know, Pt is the most widely used precious metal catalyst, but its high cost and low anti-toxic ability, which limits the application of Pt catalyst in DAFCs. In recent years, researchers have been working to explore high efficiency and lower cost catalyst materials [3–8,12]. The catalytic performance of the catalyst is usually improved by the following two methods: (1) Improve the catalytic performance of the catalyst by controlling and changing the size, morphology and various metal complexes of precious metals; (2) explore the new precious metal carrier, use the special properties of the carrier to reduce the loading of precious metals, and improve the stability and catalytic performance of the catalyst through the carrier. Therefore, finding suitable materials as carriers for noble metals to improve the stability and catalytic performance of the catalysts are urgent needed.

In recent years, due to the large specific surface area, excellent optical properties, high chemical stability and co-catalysis, semiconductor materials have received the scientist extensive attention [13,14]. The large specific surface area of the semiconductor nanomaterial provides a good carrier for the adhesion of the precious metal, improves the utilization rate of the precious metal, and thereby increasing the catalytic activity of the catalyst. Moreover, the excellent stability of semiconductor nanomaterials is beneficial to the stability of composite catalysts in DAFCs. The most important of these is that the excellent optical property of the semiconductor material makes it have a strong oxidizing ability under photoexcitation, and can oxidize the organic small

* Corresponding author.
E-mail address: zhumingshan@jnu.edu.cn (M. Zhu).

https://doi.org/10.1016/j.cclet.2020.09.049

molecules adsorbed on the surface and the intermediate products produced by the fuel cell reaction, thereby further improving the catalyst's catalytic activity and anti-toxic ability. Although the semiconductor material needs to be improved in electrical conductivity compared with the conventional noble metal or carbon carrier, the conductivity of the semiconductor material can be significantly improved by doping and changing the morphology of the semiconductor.

In 2005, Kamat's group [15] used semiconductor TiO_2 as the carrier of noble metal Pt-Ru, and successfully prepared a photocatalytic noble metal-semiconductor catalyst for direct methanol fuel cells (DMFCs) by using TiO_2 to respond to ultraviolet light. In addition, since TiO_2 is a well-known photocatalytic material, the good response of TiO_2 to ultraviolet light has successfully improved the catalytic performance of the catalyst. This research is the first time to introduce photocatalysis into a DMFC.

Benefiting from this finding, great achievements have been developed that using photoactive activity of semiconductor material as the carrier of traditional metal electrocatalyst, the electrocatalytic activity and stability of the electrocatalyst for various fuel cell reactions are greatly improved with the aid of light illumination. Therefore, it is significant to concern the overview of metal/semiconductor applied in the field of various photo-assisted fuel cell reactions. Accordingly, this review focuses on the recent progress of novel photo-responsive electrodes as the anode catalysts for improving the electrocatalytic activity of alcohol molecules oxidation under light irradiation (Scheme 1). We will gain insight into understanding the mechanism of photo&electro enhanced fuel cell reaction process, the diversified routes to construct advanced photo-responsive electrodes systems including the different photo-assisted alcohol fuel cell systems and different type of metals. Finally, the prospects of the photo-responsive electrodes for fuel cell reactions are also addressed and provided more guidance on the developing effective photo-responsive anode electrodes in fuel cell reactions and other solar energy conversion.

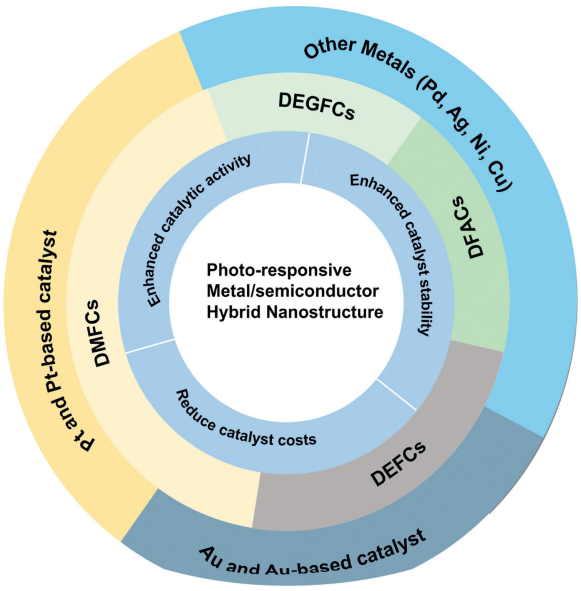

Scheme 1. Scheme of the overall content in the present review.

2. Mechanism and advantages of photo-assistant electrochemical alcohol oxidation reaction

In the photo-assisted direct alcohol fuel cells, the metal-semiconductor electrode catalyzes the alcohols oxidation is a cooperative process with photocatalysis and electrocatalysis, as shown in Scheme 2. On one hand, with the electrocatalytic processes, small organic alcohol molecules are first adsorbed on the surface of electrocatalyst, and then multi-step dehydrogenation forms carbon-containing intermediate poisoning species (COs). Then, the oxygen-containing species produced by dissociating water will react with the COs and eventually oxidize to CO_2. On the other hand, for photocatalytic processes, semiconductor materials generate photogenerated electron-hole pairs under light irradiation [16,17], and the holes in some cases also can react with OH^-/H_2O adsorbed on the semiconductor surface to form radical of $^{\bullet}OH$ [18,19]. Finally, these $^{\bullet}OH$ and holes further oxidize the small organic alcohol molecules with adsorbed on the electrode surface and the COs produced by electrocatalysis [20,21]. Therefore, the catalyst can improve catalytic oxidation performance and stability under light irradiation. Meanwhile, the corresponding electrons with photocatalytic processes were transferred to the metal and then together with the electrons from alcohol oxidation were transferred to external circuit. These electrons injections will also result in the enhancement of current.

Based on the above reaction mechanism, it is not difficult to find that the light-responsive precious metal/semiconductor electrocatalyst has obvious advantages over the traditional electrocatalyst: (1) In terms of catalytic activity, in addition to traditional electrochemical catalysis, the optical properties of semiconductor materials also play a significant catalytic role. Since the semiconductor material can generate photogenerated electron-hole pairs under the light irradiation, the strong oxidizing property of the holes can oxidize the alcohol organic small molecules, thereby photo-assisted can improve the catalytic activity of catalyst [22–27]. (2) According to the mechanism, we found that semiconductor materials can effectively improve the stability of the catalyst. This characteristic may be due to the self-cleaning performance of semiconductor materials under light conditions [20,21,24]. This is because semiconductor material can generate photogenerated electron-hole pairs under light irradiation, and these holes can oxidize the reaction intermediates and small alcoholic organic molecules adsorbed on the surface of electrocatalyst, thereby playing the role of electrode cleaning, to improve the catalytic activity and stability of the photocatalyst [21,24]. (3) The cost of catalysts directly affects the large-scale promotion of DAFCs [25]. Compared with noble metal electrocatalysts, semiconductor materials generally have lower cost and excellent stability under electrochemical environment. With the interaction of noble metal and semiconductor support, noble metal electrocatalysts can be dispersed well on the surface of support, resulting in more activate site and thereby reducing the usage of noble metal [26,27].

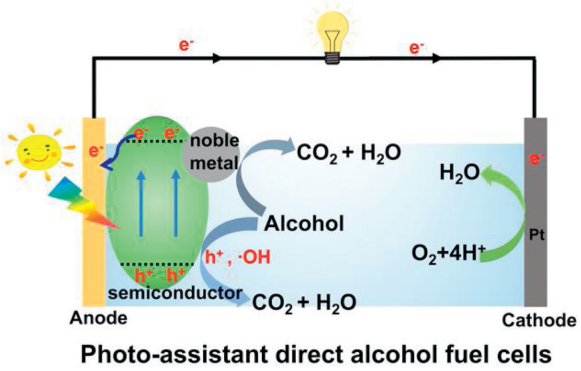

Scheme 2. Scheme for the mechanism of the photo-assistant electrochemical alcohol oxidation.

3. Different type of photo-assisted fuel cell reactions

As the descriptions in the introduction, many different types of liquid fuel such as methanol, ethanol, formic acid, and ethylene glycol have been used in photo-responsive DAFCs. Accordingly, depending on the type of small molecules, the different type of photo-assisted fuel cell reactions including methanol oxidation reaction (MOR) [15,19,26,28–73], ethanol oxidation reaction (EOR) [22,23,68,74–84], formic acid oxidation reaction (FAOR) [18,24,68,74], and ethylene glycol oxidation reaction (EGOR) [85,86].

3.1. Photo-assisted methanol oxidation reaction

Due to the advantages of higher power density, easier of fuel handling, easer storage and transportation and lower environmental impact of methanol, DMFCs have been extensively studied as promising energy conversion devices [8,87–90]. Compared to hydrogen proton exchange membranes fuel cells (PEMFCs), DMFCs with renewable liquid methanol as fuel have a unique advantage because methanol is safe for storage and transportation [8], with the methanol oxidation reaction occurring at the anode and the oxygen reduction reaction occurring at the cathode. Since the first report by using Pt-Ru electrocatalyst hybridized with TiO_2 to obtain an enhanced electrocatalytic activity and stability for MOR [15], by using semiconductor as the electrocatalyst's carrier in the improved performance of MOR attracted more and more attentions. The mechanism and pathways for this photo-assisted MOR were described in the following Eqs. 1–12 [20,21,24,52].

$$Pt + (CH_3OH)_{solution} \rightarrow Pt\text{-}(CH_3OH)_{ads} \quad (1)$$

Table 1
Recent reports on electrocatalytic activity of MOR under dark and light condition based on different photo-responsive metal/semiconductor.

Catalysts	I_{dark}	I_{light}	I_{light}/I_{dark}	Ref.
Pt-Ru/TiO_2/carbon fiber	23.3 mA/cm^2	45.0 mA/cm^2	1.93	[15]
Au/TiO_2 nanoporous	1.45 mA/cm^2	1.72 mA/cm^2	1.18	[28]
Pt/TiO_2	3.30 mA	5.70 mA	1.72	[29]
Pt-TiO_2/ITO	0.46 mA/cm^2	1.94 mA/cm^2	4.22	[30]
Pt-Ni/TNTs	24.3 mA/cm^2	37.5 mA/cm^2	1.54	[31]
Pt/TiO_2 film	0.250 mA	2.25 mA	9.00	[32]
Pt-Ru/TiO_2	20.8 mA	23.9 mA	1.15	[33]
Pt/TiO_2	5.75 mA/cm^2	8.51 mA/cm^2	1.48	[34]
Pt/TiO_2/C	870 mA/mg$_{Pt}$	1.81×10^3 mA/mg$_{Pt}$	2.08	[35]
Ni/TNT	23.8 mA/cm^2	28.3 mA/cm^2	1.19	[36]
Pt/C-Au/ZnS	234 mA/mg	412 mA/mg	1.76	[37]
Pt/TiO_2 films/B-doped diamond	3.90 mA/cm^2	5.10 mA/cm^2	1.31	[38]
Pt/WO_3/TiO_2	0.78 mA/cm^2	1.32 mA/cm^2	1.69	[39]
Pt@ZnO/Carbon cloth	2.58 mA/cm^2	3.86 mA/cm^2	1.50	[19]
PtNi/C-TNTs	108 mA/cm^2	123 mA/cm^2	1.14	[40]
Pt/RGO/TiO_2/carbon fiber	364 mA/mg	507 mA/mg	1.39	[41]
Pd/Cu_2O/graphene	718 mA/mg	1.32×10^3 mA/mg	1.84	[42]
Pt/C/TiO_2	31.0 mA/cm^2	123 mA/cm^2	3.97	[44]
Pt/TiO_2/graphene	544 mA/mg$_{Pt}$	1.35×10^3 mA/mg$_{Pt}$	2.49	[45]
Pt/TiO_2/WO_3 films	0.350 mA/cm^2	2.20 mA/cm^2	6.29	[46]
Pt/TNT/RGO	1.36 mA/cm^2	4.40 mA/cm^2	3.24	[47]
Ag@Pt/TiO_2/carbon fiber/RGO	310 mA/mg$_{Pt}$	1.50×10^3 mA/mg$_{Pt}$	4.84	[48]
Pt/SiO_2/TiO_2	0.300 mA/cm^2	0.950 mA/cm^2	3.17	[49]
Pt/C-GaOOH/Au	5.10 mA/cm^2	8.88 mA/cm^2	1.74	[50]
Pt/ZnO/graphene	957 mA/mg$_{Pt}$	1.94×10^3 mA/mg$_{Pt}$	2.02	[51]
Pt/CdS/FTO	3.60 mA/cm^2	8.64 mA/cm^2	2.40	[52]
Pt/SnO_2/graphene	612 mA/mg$_{Pt}$	1.10×10^3 mA/mg$_{Pt}$	1.80	[53]
Pt-Ag/graphene	838 mA/mg	1.84×10^3 mA/mg	2.20	[54]
Pt/g-C_3N_4	159 mA/mg$_{Pt}$	520 mA/mg$_{Pt}$	3.28	[55]
Pt/CdS/MoS_2	1.32 mA/cm^2	4.56 mA/cm^2	3.45	[57]
Pt/TiO_2/WO_3	0.510 mA/cm^2	0.700 mA/cm^2	1.37	[61]
Pt/TiO_2/Vulcan XC-72R carbon	1.21×10^3 mA/mg$_{Pt}$	3.29×10^3 mA/mg$_{Pt}$	2.71	[60]
Pt/CuI/BiOI	705 mA/mg$_{Pt}$	1.52×10^3 mA/mg$_{Pt}$	2.16	[58]
Pt/CuI/TiO_2	936 mA/mg$_{Pt}$	3.77×10^3 mA/mg$_{Pt}$	4.03	[59]
Pt/N-g-C_3N_4/ketjen black	1.75×10^3 mA/mg$_{Pt}$	2.80×10^3 mA/mg$_{Pt}$	1.60	[26]
Pt/TNTs/C	357 mA/mg$_{Pt}$	525 mA/mg$_{Pt}$	1.47	[62]
Pt/graphene/TiO_2	3.36×10^3 mA/mg$_{Pt}$	4.72×10^3 mA/mg$_{Pt}$	1.40	[63]
Pt/LTO	42.3 mA/mg$_{Pt}$	447 mA/mg$_{Pt}$	10.6	[64]
Pt/ZnO/ketjen black	432 mA/mg$_{Pt}$	964 mA/mg$_{Pt}$	2.23	[65]
Pt/g-C_3N_4/CdS	16.9 mA/mg$_{Pt}$	125 mA/mg$_{Pt}$	7.38	[56]
Pt/BiOBr	26.5 mA/mg$_{Pt}$	752 mA/mg$_{Pt}$	28.4	[66]
Pt/BiOBr	251 mA/mg$_{Pt}$	1.32×10^3 mA/mg$_{Pt}$	5.26	[67]
Pt/g-C_3N_4/MoS_2	251 mA/mg$_{Pt}$	1.62×10^3 mA/mg$_{Pt}$	6.46	[68]
Pt-Au/g-C_3N_4	1.52 mA/cm^2	2.58 mA/cm^2	1.70	[69]
Pt/Bi_2WO_6/LTO	406 mA/mg$_{Pt}$	1.41×10^3 mA/mg$_{Pt}$	3.47	[70]
Pt/Bi_2WO_6/MoS_2	1.78×10^3 mA/mg$_{Pt}$	2.74×10^3 mA/mg$_{Pt}$	1.54	[71]
Pt/BiOI/MoS_2	222 mA/mg$_{Pt}$	1.01×10^3 mA/mg$_{Pt}$	4.53	[72]
Pt/CdS quantum dots/LTO	270 mA/mg$_{Pt}$	582 mA/mg$_{Pt}$	2.16	[73]
Pd/SiO_2@TiO_2	1.57×10^3 A/mg	2.92×10^3 A/mg	1.86	[74]
Pt/ Bi_2WO_6/Cu_2S	1.85×10^3 mA/mg$_{Pt}$	5.54×10^3 mA/mg$_{Pt}$	2.99	[91]
Pt/Bi_2WO_6/RGO	936 mA/mg$_{Pt}$	1.80×10^3 mA/mg$_{Pt}$	1.92	[92]
$AgVO_3$/$LaVO_4$		0.216 mA/cm^2		[93]
BP-CNTs@PSS/AuNPs@PAH/TA	1.39 mA/cm^2	2.06 mA/cm^2	1.48	[94]
Pt-CdS/N-GQDs	167 mA/mg$_{Pt}$	741 mA/mg$_{Pt}$	4.44	[95]

$$Pt\text{-}(CH_3OH)_{ads} + OH^- \rightarrow Pt\text{-}(CH_3O)_{ads} + H_2O + e^- \quad (2)$$

$$Pt\text{-}(CH_3O)_{ads} + OH^- \rightarrow Pt\text{-}(CH_2O)_{ads} + H_2O + e^- \quad (3)$$

$$Pt\text{-}(CH_2O)_{ads} + OH^- \rightarrow Pt\text{-}(CHO)_{ads} + H_2O + e^- \quad (4)$$

$$Pt\text{-}(CHO)_{ads} \rightarrow Pt{-}CO_{ads} + H^+ + e^- \quad (5)$$

$$Pt + (OH^-)_{solution} \rightarrow Pt{-}OH_{ads} + e^- \quad (6)$$

$$Pt\text{-}(CO)_{ads} + Pt{-}OH_{ads} + OH^- \rightarrow 2\,Pt + CO_2 + H_2O + e^- \quad (7)$$

$$Semiconductor + h\nu \rightarrow Semiconductor + e_{CB}{}^- + h_{VB}{}^+ \quad (8)$$

$$h^+ + OH^- \rightarrow {}^{\bullet}OH \quad (9)$$

$$CH_3OH + {}^{\bullet}OH \rightarrow {}^{\bullet}CH_2(OH) + H_2O \quad (10)$$

$${}^{\bullet}CH_2(OH) + 5{}^{\bullet}OH \rightarrow CO_2 + 4H_2O \quad (11)$$

$$Pt\text{-}(CO)_{ads} + {}^{\bullet}OH \rightarrow Pt + CO_2 + H^+ + e^- \quad (12)$$

The recent reports on electrocatalytic MOR with and without light irradiation based on photo-responsive metal/semiconductor are summarized in Table 1 [15,19,26,28–42,44–74,91–95]. The electrocatalytic oxidation performances of methanol under light illumination are much higher than those under dark condition. It can be seen that 1.14∼28.4 times enhanced for these photo-responsive metal/semiconductor electrocatalysts under light irradiation than those of under dark condition. For example, Zhang *et al.* [30] fabricated Pt/TiO_2 nanocomposites by a sol-gel method. The electrochemical performance of Pt/TiO_2 is evaluated by studying the electrocatalytic oxidation of methanol in an alkaline medium with or without UV illumination. The electrocatalytic oxidation performance of methanol oxidation on Pt/TiO_2 under UV illumination (1.94 mA/cm^2) is about 4.2 times enhanced for the Pt/TiO_2 electrode under dark condition. Hence, electron-hole pairs generated under UV illumination could increase the conductivity of the electrode. Hu *et al.* [66] synthesized a Pt-BiOBr electrocatalyst by hydrothermal method. Then, they selected the MOR as the model reactions to evaluate its electrocatalytic properties. The peak current density of the Pt-BiOBr towards MOR is 751.7 mA/mg_{Pt}, 28.4 times higher than that under dark condition. This result indicated the excellent photoelectrocatalytic performances of the Pt-BiOBr nanocatalysts.

3.2. Photo-assisted ethanol oxidation reaction

Ethanol offers an attractive alternative as a fuel in low temperature fuel cells because it can be produced in large quantities from agricultural products and it is the major renewable biofuel from the fermentation of biomass. Based on the foregoing work [96–101], the mechanism of direct ethanol fuel cells (DEFCs) in acid solution is summarized in the following reactions: $CH_3CH_2OH \rightarrow [CH_3CH_2OH]_{ads} \rightarrow C1_{ads}$, $C2_{ads} \rightarrow CO_2$ (total oxidation), $CH_3CH_2OH \rightarrow [CH_3CH_2OH]_{ads} \rightarrow CH_3CHO \rightarrow CH_3COOH$ (partial oxidation) The formation of CO_2 goes through two adsorbed intermediates $C1_{ads}$ and $C2_{ads}$, which represent fragments with one and two carbon atoms, respectively.

As mentioned earlier, the photo-responsive metal/semiconductor catalysts are also widely used in the application of EOR [22,23,68,74–84]. The mechanism and pathways for these photo-assisted EOR were described in the following Eqs. 13–20 [82,96–101].

$$Pt + (C_2H_5OH)_{solution} \rightarrow Pt{-}(C_2H_5OH)_{ads} \quad (13)$$

$$Pt{-}(C_2H_5OH)_{ads} + 3OH^- \rightarrow Pt{-}(CH_3CO)_{ads} + 3H_2O + 3e^- \quad (14)$$

$$Pt + OH^- \rightarrow Pt{-}OH_{ads} + e^- \quad (15)$$

$$Pt{-}(CH_3CO)_{ads} + Pt - OH_{ads} \rightarrow CH_3COOH + 2\,Pt \quad (16)$$

$$Semiconductor + h\nu \rightarrow Semiconductor + e_{CB}{}^- + h_{VB}{}^+ \quad (17)$$

$$OH^- + h^+ \rightarrow {}^{\bullet}OH \quad (18)$$

$$CH_3CH_2OH + 6{}^{\bullet}OH \rightarrow 2CO_2 + 9H_2O + 6e^- \quad (19)$$

$$Intermediates(CO_{ads}) + {}^{\bullet}OH + OH^- \rightarrow CO_2 + H_2O + e^- \quad (20)$$

The recent reports on electrocatalytic EOR with and without light irradiation based on photo-responsive metal/semiconductor are summarized in Table 2. The results clearly show that the performances of electrocatalytic EOR for these photo-responsive metal/semiconductor electrocatalysts are improved 1.13–16.9 times with the aid of light illumination than those of under dark condition. For example, Hu *et al.* [83] reported a novel $Pt/BiVO_4$ electrocatalyst for EOR. In this paper, the Pt deposited $BiVO_4$ nanocomposites were obtained by photo-reduction method. For the EOR, the peak current density of $Pt/BiVO_4$ electrode was detected to be 591.3 mA/mg_{Pt} under dark condition. However, when the $Pt/BiVO_4$ electrode under visible light condition, the peak current density was enhanced 2.63 times to 1555 mA/mg_{Pt}. Obviously, the photo-responsive metal/semiconductor electrode acted as a high-efficiency electrocatalytic activity of ethanol oxidation. Jin *et al.* [77] fabricated two electrocatalysts of highly ordered Au NPs decorated bilayer TiO_2 nanotube (BTNT) and Au NPs monolayer TiO_2 nanotube (MTNT). Fig. 1 shows the illumination effect on the CV (cyclic voltammetry) tests on MTNT and BTNT decorated with Au NPs for ethanol oxidation. As shown in Figs. 1A and D, the Au/MTNT and Au/BTNT electrodes have no oxidation peaks in the absence ethanol in KOH solution, and for Figs. 1B and E, the Au/MTNT and Au/BTNT electrodes appear obvious ethanol oxidation peaks in the KOH solution with ethanol, which indicates this electrode has catalytic oxidation effect on ethanol. In addition, for Figs. 1B and E, compared with UV irradiation, Au/BTNT has greater electrocatalytic activity for EOR under visible light irradiation, and 3.6 times higher than that of Au/MTNT under visible light irradiation. Furthermore, the current density of Au/BTNT catalyzed ethanol oxidation under visible light irradiation was 1.82 times higher than that under dark conditions. The Au/BTNT electrode performs excellent ethanol electro-oxidation

activity under visible light illumination because of the plasmon-induced charge separation and the enhanced visible light harvesting.

3.3. Photo-assisted formic acid oxidation reaction

Formic acid as a liquid fuel can provide quite high power density and a high theoretical open circuit voltage under formic acid-ambient air cell operation even at room temperature [102]. Hence, the electro-oxidation property of formic acid can be more rapidly compare to ethanol. It also has low fuel crossover through the Nafion membrane while compared to DMFC which face a big problem of methanol crossover. This is due to the repulsion between $HCOO^-$ in formic acid and sulfuric group in the surface of Nafion membrane [96,97]. In addition, formic acid as a strong electrolyte can be expected to facilitate both electronic and proton transport within the anode compartment of the fuel cell [103]. Therefore, the photo-responsive direct formic acid fuel cells (DFAFCs) are also a research hotspot today. The mechanism and pathways for these photo-assisted FAOR are described in the following Eqs. 21–27 [68,104].

$$Pt + (HCOOH)_{solution} \rightarrow Pt\text{-}(HCOOH)_{ads} \quad (21)$$

$$Pt\text{-}(HCOOH)_{ads} + OH^- \rightarrow Pt{-}HCOO_{ads} + H_2O + e^- \quad (22)$$

$$Pt{-}HCOO_{ads} \rightarrow Pt + CO_2 + H^+ + e^- \quad (23)$$

$$Semiconductor + h\nu \rightarrow Semiconductor + e_{CB}{}^- + h_{VB}{}^+ \quad (24)$$

$$OH^- + h^+ \rightarrow {}^{\bullet}OH \quad (25)$$

$$HCOOH + 2{}^{\bullet}OH \rightarrow CO_2 + 2H_2O + e^- \quad (26)$$

$$Intermediates\ (CO_{ads}) + {}^{\bullet}OH \rightarrow CO_2 + H^+ + e^- \quad (27)$$

The recent reports on electrocatalytic activity of FAOR with and without light irradiation based on photo-responsive metal/semiconductor are summarized in Table 3. The results indicate that the performances of electrocatalytic FAOR for these photo-responsive metal/semiconductor electrocatalysts are improved 1.41–4.50 times with the aid of light illumination than those of under dark condition. For example, Subramanian's group [18] reported an anode catalyst Pt/TNT of formic acid oxidation. Formic acid electrooxidation is evident from the characteristic peak observed in the voltammogram. In the forward scan of Pt/TNT, the anodic peak is noted at 0.60 V. In the reverse scan, the characteristic peak is noted at 0.42 V. The current density of Pt/TNT electrode for FAOR was 72 mA/cm^2 in the presence of UV illumination, which showed 4.5-folds increase comparison with that of absence UV illumination. This result was attributed to the Pt/TNT catalyzed FAOR under UV illumination that a synergistic reaction between electrocatalysis and photocatalysis.

3.4. Photo-assisted ethylene glycol oxidation reaction and others

Ethylene glycol (EG) is safer than the other alcohols due to the fact that EG has lower toxicity, higher ignition point (418 °C) and boiling point (198 °C) [105–107]. Meanwhile, the complete oxidation of EG delivers $10e^-$ compared with $6e^-$ by methanol [10], and the theoretical power capacity of EG is provided about 4.8 Ah/mL, which is much higher than methanol (4 Ah/mL) [108]. These advantages endow EG as the renewable fuel in the low temperature DAFCs. The mechanism and pathways for these photo-assisted EGOR were described in the following Eqs. 28–12 [86].

$$Pt + (CH_2OH)_{2solution} \rightarrow Pt\text{-}(CH_2OH)_{2ads.} \quad (28)$$

$$Pt\text{-}(CH_2OH)_{2ads} + 4OH^- \rightarrow Pt\text{-}(HCO)_{2ads} + 4H_2O + 4e^- \quad (29)$$

$$Pt\text{-}(HCO)_{2ads} + 4OH^- \rightarrow Pt\text{-}(HCOO)_{2ads} + 2H_2O + 4e^- \quad (30)$$

$$Pt{-}HCOO_{ads} + e^- \rightarrow Pt{-}CO_{ads} + OH^- \quad (31)$$

$$Pt\text{-}(HCO)_{ads} + e^- \rightarrow Pt{-}CO_{ads} + OH^- \quad (32)$$

$$Pt{-}OH^- \rightarrow Pt + OH_{ads} + e^- \quad (33)$$

$$Pt{-}CO_{ads} + Pt + OH_{ads} \rightarrow 2Pt + CO_2 + H^+ + e^- \quad (34)$$

Table 2
Recent reports on electrocatalytic activity of EOR under dark and light condition based on different photo-responsive metal/semiconductor.

Catalysts	I_{dark}	I_{light}	I_{light}/I_{dark}	Ref.
$PtNiRu/TiO_2$	9.90 mA/cm^2	24.6 mA/cm^2	2.48	[22]
Au/TNT		1.06 mA		[74]
Au nanowires/mZnO	0.840 mA/mg_{Au}	1.85 mA/mg_{Au}	2.20	[23]
$Pt/Fe_2O_3/C$	31.1 mA/cm^2	35.2 mA/cm^2	1.13	[75]
Au nanowire/rGO/TiO_2	9.30 mA/cm^2	15.0 mA/cm^2	1.61	[76]
Au NPs/TNT	0.610 mA/cm^2	1.11 mA/cm^2	1.82	[77]
Pt NPs/rGO/CdS	1.12 mA/cm^2	3.63 mA/cm^2	3.24	[78]
ZnO@Pd@Pt holl nanorods	6.80 mA/cm^2	8.20 mA/cm^2	1.21	[79]
Au/CuI	101 mA/mg_{Au}	561 mA/mg_{Au}	5.55	[80]
NiFe/ZrO_2/n-Si	13.6 mA/cm^2	34.4 mA/cm^2	2.53	[81]
Pt/BiOI	293 mA/mg_{Pt}	874 mA/mg_{Pt}	2.99	[82]
$Pt/BiVO_4$	591 mA/mg_{Pt}	1.55×10^3 mA/mg_{Pt}	2.63	[83]
Pt/g-C_3N_4/BiOI	37.0 mA/mg_{Pt}	625 mA/mg_{Pt}	16.9	[84]
Pt/g-C_3N_4/MoS_2	76.9 mA/mg_{Pt}	166 mA/mg_{Pt}	2.15	[68]
BP-CNTs@PSS/AuNPs@PAH/TA	0.660 mA/cm^2	1.09 mA/cm^2	1.65	[94]
Pt-CdS/N-GQD	119 mA/mg_{Pt}	251 mA/mg_{Pt}	2.11	[95]

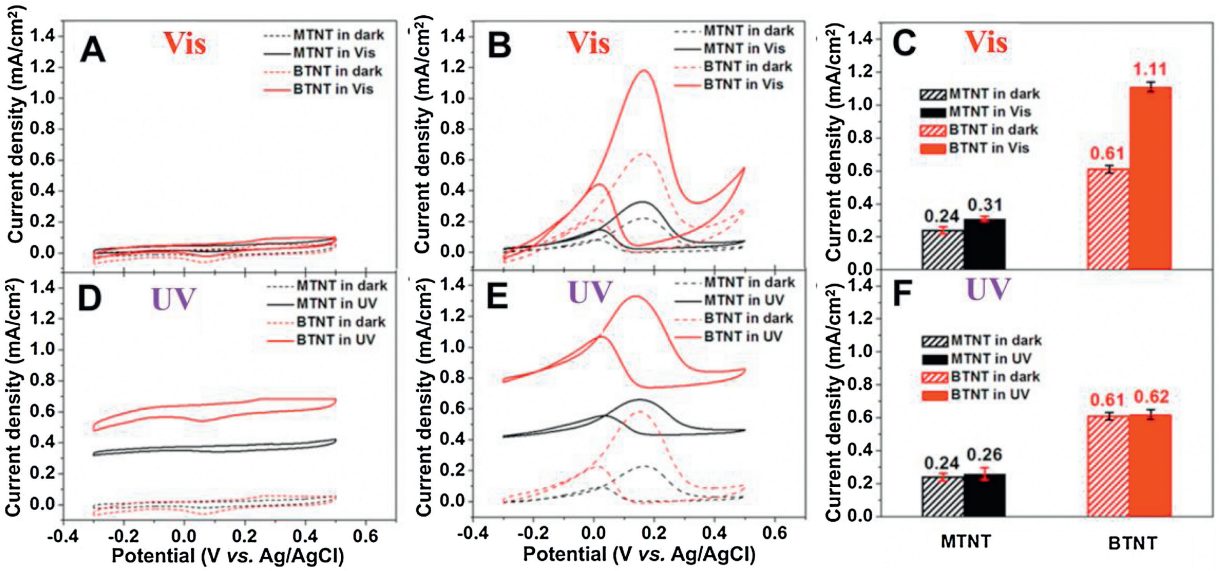

Fig. 1. Effect of illumination to the CVs measured (A, D) in the absence of and (B, E) in the presence of 1 mol/L ethanol in 1 mol/L KOH. (C, F) Corresponding statistic histograms of ethanol electro-oxidation peak currents. Scanning rate is 50 mV/s. Copied with permission [77]. Copyright 2011, Elsevier B.V.

Table 3
Recent reports on electrocatalytic activity of FAOR under dark and light condition based on different photo-responsive metal/semiconductor.

Catalysts	I_{dark}	I_{light}	I_{light}/I_{dark}	Ref.
Pt NPs/TNT	10.2 mA/cm^2	14.4 mA/cm^2	1.41	[24]
Au/g-C_3N_4	4.71 mA/cm^2	9.43 mA/cm^2	2.00	[74]
Pt/TNT	16.0 mA/cm^2	72.0 mA/cm^2	4.50	[18]
Pt/g-C_3N_4/MoS_2	624 mA/mg$_{Pt}$	1.56×10^3 mA/mg$_{Pt}$	2.50	[68]
Pt-CdS/N-GQDs	1.05×10^3 mA/mg$_{Pt}$	2.41×10^3 mA/mg$_{Pt}$	2.29	[95]

$$\text{Semiconductor} + h\nu \rightarrow \text{Semiconductor} + e_{CB}^- + h_{VB}^+ \quad (35)$$

$$OH^- + h^+ \rightarrow {}^{\bullet}OH \quad (36)$$

$$(CH_2OH)_2 + 10{}^{\bullet}OH \rightarrow 2CO_2 + 8H_2O + 5e^- \quad (37)$$

$$\text{Intermediates } (CO_{ads}) + {}^{\bullet}OH \rightarrow CO_2 + H^+ + e^- \quad (38)$$

Similar to the above phenomena, by using semiconductor as the metal electrocatalysts carrier, the performances of electrocatalytic EGOR are improved 1.71–4.20 times with the aid of light illumination than those of under dark condition. For example, Gao *et al.* [85] reported that two-dimensional (2D) bismuth tungstate (Bi_2WO_6) nanosheets worked as the carriers for deposition of Pt NPs as the anode catalysts in the application of EGOR. Attributed to the excellent absorption property of Bi_2WO_6 in visible light, Pt/Bi_2WO_6 electrode shows enhanced catalytic activity and stability towards visible light illumination. The current density by using Pt/Bi_2WO_6 electrode is reached to 492.5 mA/mg$_{Pt}$ with visible light illumination, which is about 4.2 times higher than the same electrode in dark condition.

Besides the above small alcohol molecules, some other carbohydrate such as photo-assistant electrocatalysis lactose oxidation reaction (LOR) [109] and galactose oxidation reaction (GOR) [110] obtains a very high interest. For example, Hosseini's group [105] fabricated a Pt NPs-decorated TNT (Pt/TNT) electrode by a microemulsion method. Pt/TNT has larger oxidation peak currents than a smooth platinum electrode for GLOR. This result confirmed the better electrocatalytic activity than the traditional Pt electrode. Additionally, the peak current density of GLOR on Pt/TNT was achieved at 13.5 mA/cm^2 with UV illumination. However, the peak current density of GLOR on Pt/TNT only reached 6.10 mA/cm^2. Moreover, the Pt/TNT electrode exhibits a self-cleaning ability by being exposed to UV light, allowing the Pt/TNT electrode to be used repeatedly. These results are mainly attributed to the excellent photo-response and self-cleaning properties of TiO_2 semiconductor materials to UV light.

The recent reports on electrocatalytic activity of EGOR, LOR and GLOR with and without light irradiation based on photo-responsive metal/semiconductor are summarized in Table 4. The results indicate that the performances of electrocatalytic EGOR, LOR and GLOR for these photo-responsive metal/semiconductor electrocatalysts are improved 1.71–4.20 times with the aid of light illumination than those of under dark condition.

Based on the above mechanism, photo-responsive metal/semiconductor catalysts catalyze the oxidation of alcohols have the following two things in common: (1) Both are electrocatalytic and photocatalytic co-catalytic oxidation reactions; (2) all final products of oxidation are environmentally friendly gas of CO_2.

4. Different kind of metals in photo-responsive metal/semiconductor hybrid nanostructure

4.1. Pt and Pt-based catalyst

Precious metal Pt is considered as one of the preeminent catalysts for DAFCs because of its perfect catalytic activity of organic small molecule. However, from the above-mentioned reaction mechanism of alcohol oxidation, it can be seen that the intermediate products produced by alcohol oxidation can be adsorbed on the surface of Pt, occupying the reaction site of Pt, which leads to a severe decrease in reaction kinetics [3]. To address the poisoning by CO_{ads}, modification of Pt with foreign materials (*e.g.*, semiconductor and other metals) is necessary.

For example, Li *et al.* [29] used $H_2PtCl_6 + H_2SO_4$ aqueous solution as the precursors, through the current static chronopotentiometry

method, electrodeposited Pt nanoparticles on the surface of a highly ordered TNT array. Under the irradiation of ultraviolet light, current of the novel catalyst increased by 58% compared to that without illumination for methanol oxidation. Zhang *et al.* [30] successfully prepared the Pt/TiO_2 electrode by a sol-gel method and Pt nanoparticles with the average size 2.6 nm were well uniformly dispersed on porous TiO_2. The catalytic activity of methanol oxidation was studied in an alkaline medium under ultraviolet light irradiation, and the results shown that the electrochemical performance and poisoning resistance of Pt-TiO_2 electrode were markedly improved under UV illumination. Zhu's group [55] deposited ultrasmall Pt nanoclusters on ultrathin two dimensional g-C_3N_4 nanosheet through a simple reflux method with ethanol as the reducing agent. The average size of Pt nanocluster is about 3.2 nm (Fig. 2). The as-prepared Pt/g-C_3N_4 modified electrode exhibited higher performance of methanol oxidation reaction upon visible light irradiation compared to the traditional ambient electrocatalytic oxidation. Therefore, pure Pt catalysts have greatly improved their catalytic performance and stability through the optimization and improvement by semiconductor materials under light irradiation.

In order to further improve the catalytic activity, stability and decrease the cost of Pt catalysts, the introduction of other metals is the most promising strategy for photo-responsive fuels cell reactions [15,31,33,40,42,43,79,111,112]. For example, Zhang's group [31] dispersed Pt-Ni nanoparticles on highly ordered TNTs arrays *via* pulse electrodeposition method and then investigated the catalytic activities and stability of Pt-Ni/TNTs electrode for methanol electro-oxidation in alkaline media both in the dark and under illumination. The result shows that Pt-Ni/TNTs electrode possessed better catalytic activities and stability for methanol oxidation than Pt/TNTs electrode under the same condition.

4.2. Au and Au-based catalyst

By the same token, Au as a precious metal and a common catalyst also has received the attention of researchers. Meanwhile, many efforts have been made to enhance the activity and stability of Au-based electrocatalysts [77]. For example, Hsu's group [37] synthesized a novel Au/ZnS core/shell nanocrystals with controllable shell thicknesses. In the process, Au nanoparticles with an average diameter of 18 nm were first prepared. Then Au/ZnS nanocrystals with well-defined core/shell architecture were prepared using the cysteine-assisted hydrothermal method. By increasing the concentrations of Au nanoparticles, the shell thickness of Au/ZnS decreased obviously (Fig. 3). Then the photocatalytic properties of Au/ZnS core/shell nanocrystals toward methanol oxidation were studied and the results showed that incorporation of Au/ZnS nanocrystals to Pt/C catalyst not only enhanced the current density of methanol oxidation, but also resolved the CO poisoning issue generated in the process of methanol oxidation. Ramaraj *et al.* [112] prepared the amine-functionalized EDAS (*N*-[3-(trimethoxysilyl)propyl]ethylenediamine) silicate sol-gel supported core-shell TiO_2-Au nanoparticles (EDAS/$(TiO_2\text{-}Au)_{nps}$) by $NaBH_4$ reduction of $HAuCl_4$ precursor on preformed TiO_2 nanopaticles in the presence of EDAS monomer.

Table 4
Recent reports on electrocatalytic activity of EGOR, LOR and GLOR under dark and light condition based on different photo-responsive metal/semiconductor.

Catalysts	I_{dark}	I_{light}	I_{light}/I_{dark}	Ref.
Pt/Bi_2WO_6	117 mA/mg_{Pt}	493 mA/mg_{Pt}	4.20	[85]
Pd/Cu_2S	1.89×10^3 mA/mg_{Pd}	3.26×10^3 mA/mg_{Pd}	1.72	[86]
Pt/TNT	6.10 mA/cm^2	13.5 mA/cm^2	2.21	[110]
Pt/TNT/Ti	1.48 mA/cm^2	2.53 mA/cm^2	1.71	[109]

The EDAS/$(TiO_2\text{-}Au)_{nps}$ (TiO_2:Au = 100:1) electrodes showed 223 times increase in the photocurrent when compare to the Jin's group [113] reported the photoelectrochemical oxidation of methanol at TiO_2 nanotube (TNT) modified electrode. Hence, the EDAS/$(TiO_2\text{-}Au)_{nps}$ photoelectrocatalyst both have excellent catalytic performance and greatly save the amount of precious metals.

In addition, Au-based electrocatalyst has also attracted by their outstanding surface plasmon resonance (SPR) properties, which great enhance the optical activity electrocatalysts [114]. However, the rapid recombination of photogenerated electrons and holes reduces the effect of SPR [115]. Accordingly, combining Au NPs with semiconductor materials can transfer excited hot electrons to the conduction band (CB) of adjacent semiconductors to prevent the recombination of hot electrons and holes, which is defined as plasmon-induced charge separation [115,116]. There are many studies on this principle in photo-assisted DAFCs. For example, Chang *et al.* [74]. reported that the Au/g-C_3N_4 composite material obtained by supporting Au NPs on g-C_3N_4 was used as a photoelectrocatalyst for FAOR. Au/g-C_3N_4 nanocomposite possesses significantly enhanced photoelectrocatalytic activity under UV light illumination, compared with pure g-C_3N_4 and Au NPs. UV–vis spectrum of Au/g-C_3N_4 shows two distinct peaks at 440 and 525 nm, corresponding to the absorption edge of g-C_3N_4 and the surface plasmon resonance absorption peak of Au NPs, respectively. That is why Au/g-C_3N_4 nanocomposite possesses significantly enhanced photoelectrocatalytic activity under light illumination, compared with pure g-C_3N_4 and Au NPs. Therefore, the synergic effect of Au NPs SPR and g-C_3N_4 is responsible for the superior photoelectrocatalytic performance and is effective to mitigate the surface-poisoning species.

On the other hand, the SPR of Au NPs effectively improves the light utilization efficiency of Au NPs/semiconductor composite materials. For example, Sun *et al.* [80] reported that Au NPs were loaded on CuI particles by photo-reduction method. The absorption edge of CuI was observed at *ca.* 406 nm. Due to the SPR characteristics of Au nanoparticles, a broad SPR absorption centered at 490 nm was observed in the composite of Au/CuI. The SPR absorption in visible region makes the as-prepared Au/CuI composite catalytically active under visible-light irradiation, which effectively improves the utilization of light by composite materials. Moreover, the activity of Au/CuI for EOR was reached 561 mA/mg_{Au} under visible light iradiation, which was 5.6 times that in the absence of light.

Additionally, SPR can create sharp spectral absorption in the visible region [117–119] and the excited plasmon resonances can greatly enhance the catalytic activity by the enhancement of electric field near the nanocrystal surface [120–124]. Therefore, Au can also be used as a support for other precious metals in light-assisted DAFCs due to its SPR property [125–132]. For example, Xu *et al.* [127] reported a facile method for the prepared of 3D dendritic core-shell PtAu@Pt nanocrystals (NC), which can provide higher photoelectrocatalystic activity both in methanol and ethanol oxidation reaction than Pt/C due to the plasma effect from plasmonic Au nanoparticles. In addition, compared with Pt/C catalysts, PtAu@Pt electrode catalyzed the oxidation of methanol and ethanol under visible light irradiation had a larger electrochemically active surface area due to the plasma effect of Au NPs.

Chen *et al.* [132] reported an anisotropic Pt-edged Au nanodisks that were synthesized by controlling overgrowth of Pt on edges of Au nanodisks (Pt-edged Au NDs) as catalyst for plasmon-enhanced electrochemical methanol oxidation reaction under visible-NIR light illumination, showing greatly enhanced electrochemical activity by SPR (Fig. 4). This study presented the first investigation on plasmon-boosted electrochemical reaction in visible and NIR region. From Fig. 4C, the SPR of the Pt-edged Au NDs electrode was entirely caused by Au NDs, and no plasma effect was observed on

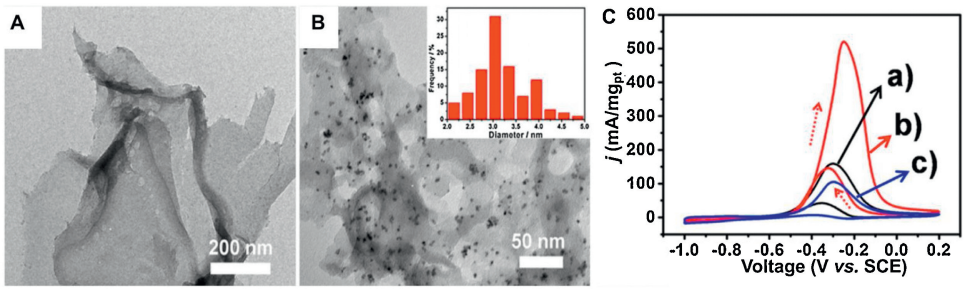

Fig. 2. Transmission electron microscope (TEM) images of ultrathin g-C_3N_4 nanosheets (A) and Pt/g-C_3N_4 nanocomposites (B). The insert is the size distribution of Pt NPs in Pt/g-C_3N_4. (C) CVs of the Pt/g-C_3N_4 under dark (a) and visible light illumination (b), and pure Pt NPs (c) in 1.0 mol/L CH_3OH +1.0 mol/L KOH solution. Copied with permission [55]. Copyright 2016, Elsevier B.V.

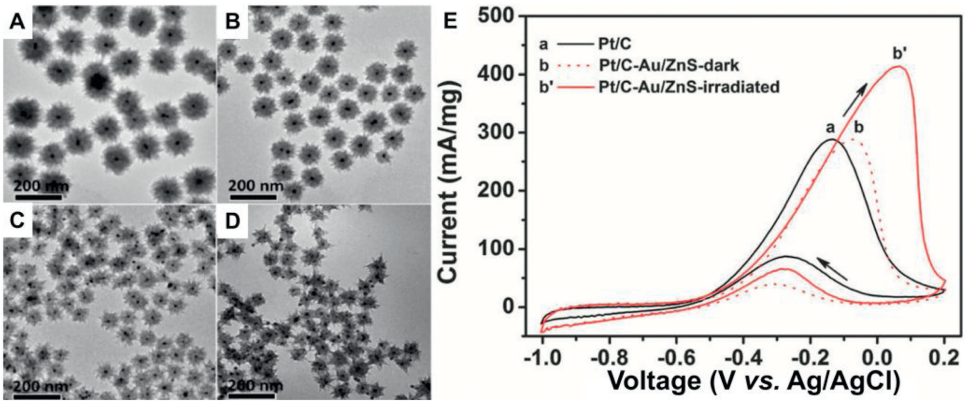

Fig. 3. TEM images of Au/ZnS nanocrystals prepared with Au of (A) 22.5, (B) 45, (C) 90 and (D) 180 mmol/L. (E) CVs of methanol oxidation on pristine Pt/C and composite Pt/C-Au/ZnS-1 catalysts under different measurement conditions. Copied with permission [37]. Copyright 2013, the Royal Society of Chemistry.

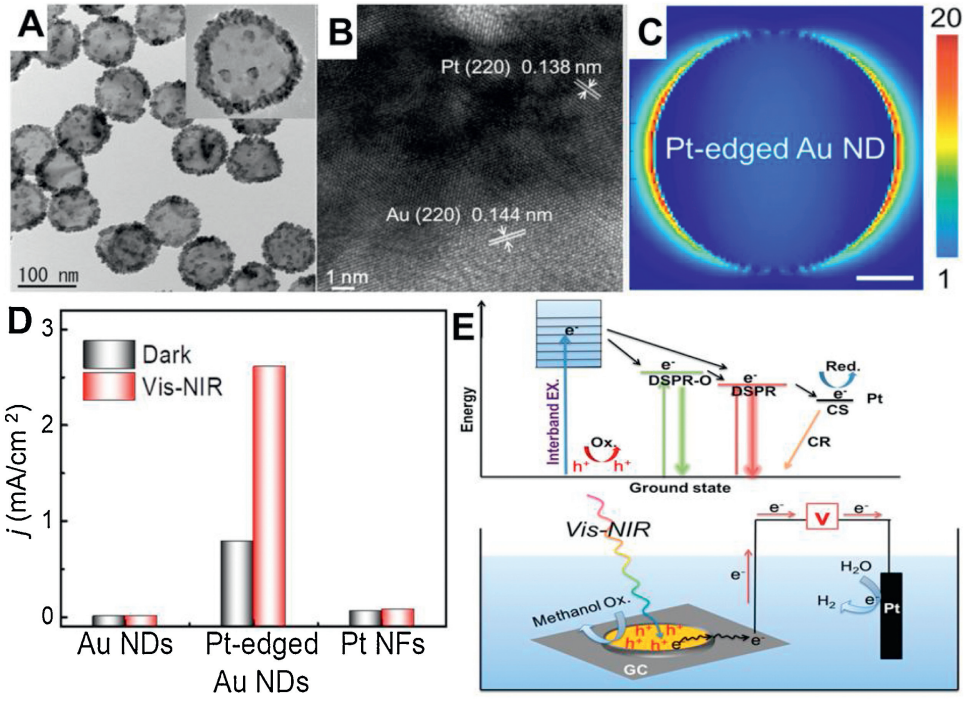

Fig. 4. (A) TEM and (B) high resolution TEM (HRTEM) images of Pt-edged Au NDs. (C) Finite-difference-time-domain (FDTD) simulated plasmon-induced electrical field distribution on Pt-edged Au ND. (D) MOR peak intensity over different catalysts on Visible-NIR light illumination and dark condition. (E) Schematic diagram for radiative decay of SPR excitation (above) and reaction mechanism for MOR over Pt-edged Au NDs (below). Copied with permission [132]. Copyright 2019, the Royal Society of Chemistry.

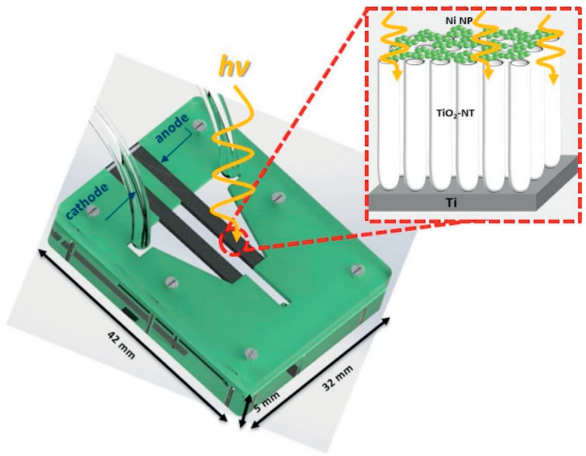

Fig. 5. Schematic representation of the microfluidic fuel cell. (Ti/TNT/Ni as anode and Pt/toray paper as cathode) that uses methanol fuel and O_2 dissolved oxidant. Microfluidic fuel cell volume of 6.72 cm^3. Copied with permission [134]. Copyright 2016, Elsevier Ltd.

Pt. Fig. 4D shows that the electrocatalytic activity of the Pt-edged Au NDs electrode to catalyze the methanol oxidation has been significantly improved due to the plasma effect of Au NDs under visible-NIR irradiation. From Fig. 4E, we can see that Pt nanoparticles can also be used as a good conductor, which can charge-separate the hot electrons that generate plasma effect under the illumination of Au NDs, leaving more active hot holes on the surface for methanol oxidation. Therefore, combining Au with other precious metals and using Au plasma effect can effectively improve the catalytic activity of the catalyst under light, which is also a focus of research on photo-assisted DAFCs in recent years.

4.3. Other metals catalysts (Pd, Ag, Ni, Cu)

Although Pt and Au metal catalysts are considered to be the best electrocatalysts in direct alcohol fuel cells (DFACs), the high cost of Pt and Au affects their wide application in electrocatalysis. Therefore, the search for other metal materials especially with low price and high catalytic activity is also the focus of scientist research in recent years. For example, Pd [86], Ag [133], Ni [36,134], Cu [135] and other metals [136] have also been extensively studied in DAFCs in recent years.

For example, Lin *et al.* [51] used a simple method to deposit Pd onto the surface of ZnO/graphene nanosheets to form a new catalyst. The catalyst has obvious catalytic activity with photo-electrooxidation methanol under the irradiation of ultraviolet light and visible light, reaching 733.5 mA/mg (UV irradiation) and 818.3 mA/mg (visible irradiation), respectively. Lim *et al.* [133] found that silver deposited titania (Ag/TiO_2) nanocomposite thin films were fabricated by the simple sonochemical deposition of Ag on preformed aerosol-assisted chemical vapor deposited TiO_2 thin films. The Ag/TiO_2-modified photoelectrode showed a photocurrent density of 1 mA/cm^2, which is 4.0 times that of an unmodified TiO_2 photoelectrode. The modification of Ag on the TiO_2 surface significantly enhanced the photoelectrocatalytic performance by improving the interfacial charge transfer processes, which minimized the charge recombination.

Furthermore, as shown in Fig. 5, Arriaga's group [134] reported that an anodic photo-electrocatalyst comprising anodically grown TNT with an average inner diameter of 70 nm and lengths of 7, 15 and 30 μm with nanoparticulate electrodeposited Ni species were synthesized and evaluated for its use as anode for direct methanol fuel cell. UV–vis irradiation coming from a Xe lamp on the anodes increased the current density by 24% in half-cell configuration. Finally, a microfluidic fuel cell was assembled and tested using methanol as fuel reached an over current protection of 0.7 V. This finding suggests that such composite materials are promising alternatives for the development of a new generation of hybrid-microfluidic devices.

In addition, on the basis of controlling the cost and higher catalytic activity, researchers have also prepared alloy/semiconductor catalysts combining two or more base metals [136]. Liu's group [136] reported $NiFe/ZrO_2$/n-Si photoanodes with efficient photoelectrocatalytic activity for ethanol oxidation reaction (EOR) in alkaline medium (1.0 mol/L KOH). From Fig. 6, $NiFe/ZrO_2$/n-Si electrode exhibited apparently improved EOR activity with the mass-specific activity of 34.4 mA/cm^2 under visible light illumination, which is approximately 2.53 times higher than that in the dark (13.6 mA/cm^2). $NiFe/ZrO_2$/n-Si electrode presented obviously enhanced stability under visible light illumination due to the acceleration of the oxidation of intermediate products adsorbed on the surface of the catalyst

5. Conclusions and future outlook

In summary, this paper outlines the advantages of recent applications of light-responsive precious metal/semiconductor electrodes in DAFCs, several DAFCs research advances, types of precious metal catalysts. The new semiconductor materials as carriers not only reduce the loading capacity of precious metals, but also improve the catalytic activity and stability of catalysts. Although the electrical conductivity of semiconductor materials is comparison with the traditional precious metals or carbon carrier needs to be improved, the photo-responsive metal/semiconductor electrode has unique optical and electrical properties. Besides, the synergistic effect of photocatalysis and electrocatalysis for alcohol,

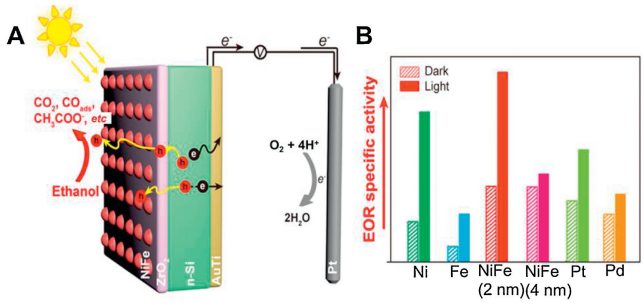

Fig. 6. (A) Schematic of a possible mechanism for the photo-assisted ethanol oxidation process for $NiFe/ZrO_2$/n-Si photoanode under visible light illumination. (B) The histogram of EOR oxidation current density for various Si photoanodes with and without visible light illumination. Copied with permission [136]. Copyright 2018, American Chemical Society.

and the strong oxidation ability of holes from the exciting semiconductor material under the light illumination make the electrode have the obvious self-cleaning ability. Compared with traditional noble metal anode electrocatalysts, these synergistic effects between metal and semiconductors show great potential in the design of a new generation of DAFCs with the aid of solar energy.

Although great progresses have been obtained on the application of photo-responsive metal/semiconductor electrode in various fuel cell reactions, further researches still need to be considered. (1) The innovation of simply synthetic methods. To extend the fundamental research in practical application, a green, pollution-free, simple, controllable, low-cost and large-scale preparation method should be considered. (2) The selection of catalyst carrier. Different semiconductor has different optical, electrical, and oxidative properties, the suitable semiconductors and their composites for different kind of alcohol oxidation need to be selected. (3) The in-depth exploration of synergistic mechanism. Although the phenomena on the improved activity and stability by using photo-responsive metal/semiconductor electrodes with the aid of solar light illumination were confirmed by solidly results, the *in-situ* charge transfer in photo- and electro-catalytic process and the oxidation pathways of alcohol molecules should be given more clear proofs. (4) Extending to other electrochemical applications. Taking the advantage of the semiconductor (*viz.* semiconductor can harvest solar energy to the chemical energy and further to be transformed into electric and other forms properties), the researchers can extend the photo-response metal/semiconductor electrodes to other electrochemical areas such as electroanalysis, bioelectrochemistry, supercapacitor, battery and so on. In conclusion, with the development of science and technology, we will have more opportunities to design more effective photo-responsive metal/semiconductor composite electrode, thus laying a solid foundation for large-scale application of the new generation of fuel cells.

Declaration of competing interest

The authors declare no conflict of interest.

Acknowledgments

The authors appreciate to the National Natural Science Foundation of China (Nos. 21603111, 51702173), Guangdong Basic and Applied Basic Research Foundation (No. 2020B1515020038), and the Pearl River Talent Recruitment Program of Guangdong Province (No. 2019QN01L148).

References

[1] A.S. Arico, S. Srinivasan, V. Antonucci, Fuel Cells 1 (2001) 133–161.
[2] X. Zhao, M. Yin, L. Ma, et al., Energ. Environ. Sci. 4 (2011) 2736–2753.
[3] N. Kakati, J. Maiti, S.H. Lee, et al., Chem. Rev. 114 (2014) 12397–12429.
[4] J.M. Andujar, F. Segura, Renew. Sust. Energ. Rev. 13 (2009) 2309–2322.
[5] M.N. Cao, D.S. Wu, R. Cao, ChemCatChem 6 (2014) 26–45.
[6] S. Sharma, B.G. Pollet, J. Power Sources 208 (2012) 96–119.
[7] E. Antolini, Appl. Catal. B: Environ. 100 (2010) 413–426.
[8] H.S. Liu, C.J. Song, L. Zhang, et al., J. Power Sources 155 (2006) 95–110.
[9] H.R. Yue, Y.J. Zhao, X.B. Ma, J.L. Gong, Chem. Soc. Rev. 41 (2012) 4218–4244.
[10] H.J. Kim, S.M. Choi, S. Green, et al., Appl. Catal. B: Environ. 101 (2011) 366–375.
[11] Y. Liu, C. Luo, H.C. Liu, Angew. Chem. Int. Ed. 51 (2012) 3249–3253.
[12] A.S. Moura, J.L.C. Fajin, M. Mandado, M. Cordeiro, Catalysts 7 (2017) 20.
[13] M. Abdullah, S.K. Kamarudin, Renew. Sust. Energ. Rev. 76 (2017) 212–225.
[14] C.M. Suarez, S. Hernández, N. Russo, Appl. Catal. A: Gen. 504 (2015) 158–170.
[15] K. Drew, G. Girishkumar, K. Vinodgopal, P.V. Kamat, J. Phys. Chem. B 109 (2005) 11851–11857.
[16] A.L. Linsebigler, G. Lu, J.T. Yates, Chem. Rev. 95 (1995) 735–758.
[17] J. Schneider, M. Matsuoka, M. Takeuchi, et al., Chem. Rev. 114 (2014) 9919–9986.
[18] N. Mojumder, S. Sarker, S.A. Abbas, Z. Tian, V. Subramanian, ACS Appl. Mater. Interfaces 6 (2014) 5585–5594.
[19] C. Su, Y. Hsueh, C. Kei, C. Lin, T. Perng, J. Phys. Chem. C 117 (2013) 11610–11618.
[20] Y. Song, Z. Gao, P. Schmuki, Electrochem. Commun. 13 (2011) 290–293.
[21] M.G. Hosseini, M.M. Momeni, Electrochim. Acta 70 (2012) 1–9.
[22] D. Chu, S. Wang, P. Zheng, et al., ChemSusChem 2 (2009) 171–176.
[23] A. Leelavathi, G. Madras, N. Ravishankar, J. Am. Chem. Soc. 136 (2014) 14445–14455.
[24] M.G. Hosseini, M.M. Momeni, Fuel Cells 12 (2012) 406–414.
[25] E. Antolini, Appl. Catal. B: Environ. 181 (2016) 298–313.
[26] J. Cheng, X. Hu, J. Zhang, et al., J. Mater. Sci. 52 (2017) 8444–8454.
[27] C. Zhai, M. Sun, Y. Du, J. Inorg. Mater. 32 (2017) 897–903.
[28] C. Jia, H. Yin, H. Ma, et al., J. Phys. Chem. C 113 (2009) 16138–16143.
[29] Z. Li, X. Cui, Y. Lin, J. Nanosci. Nanotechnol. 9 (2009) 2297–2302.
[30] H. Zhang, W. Zhou, Y. Du, et al., Int. J. Hydrogen Energ. 35 (2010) 13290–13297.
[31] H. He, P. Xiao, M. Zhou, et al., Catal. Commun. 16 (2011) 140–143.
[32] S. Wu, J. He, J. Zhou, et al., J. Mater. Chem. 21 (2011) 2852–2854.
[33] A.S. Polo, M.C. Santos, R.F. Souza, W. Alves, J. Power Sources 196 (2011) 872–876.
[34] C. Lin, H. Huang, J. Yang, M. Shao, Microelectron. Eng. 88 (2011) 2644–2646.
[35] W. Li, Y. Bai, F. Li, et al., J. Mater. Chem. 22 (2012) 4025–4031.
[36] H. He, P. Xiao, M. Zhou, et al., Int. J. Hydrogen Energ. 37 (2012) 4967–4973.
[37] W. Chen, Y. Lin, T. Yang, Y.C. Pu, Y.J. Hsu, Chem. Commun. 49 (2013) 8486–8488.
[38] T. Spataru, M. Marcu, N. Spataru, Appl. Surf. Sci. 269 (2013) 171–174.
[39] C. Wang, F. Jiang, R. Zhou, et al., Mater. Res. Bull. 48 (2013) 1099–1104.
[40] H. He, P. Xiao, M. Zhou, et al., Electrochim. Acta 88 (2013) 782–789.
[41] C. Wang, F. Jiang, R. Yue, H. Wang, Y. Du, J. Solid State Electr. 18 (2014) 515–522.
[42] L. Ye, Z. Li, X. Zhang, F. Lei, S. Lin, J. Mater. Chem. A 2 (2014) 21010–21019.
[43] D.V. Arulmani, J.I. Eastcott, S.G. Mavilla, E.B. Easton, J. Power Sources 247 (2014) 890–895.
[44] J. Huang, J. Zang, Y. Zhao, L. Dong, Y. Wang, Mater. Lett. 137 (2014) 335–338.
[45] L. Ye, Z. Li, L. Zhang, F. Lei, S. Lin, J. Colloid Interface Sci. 433 (2014) 156–162.
[46] T. Wang, J. Tang, S. Wu, X. Fan, J. He, J. Power Sources 248 (2014) 510–516.
[47] C. Zhai, M. Zhu, D. Bin, et al., ACS Appl. Mater. Interfaces 6 (2014) 17753–17761.
[48] C. Wang, R. Yue, H. Wang, et al., Int. J. Hydrogen Energ. 39 (2014) 5764–5771.
[49] X. Fan, C. Zhang, H. Xue, et al., RSC Adv. 5 (2015) 78880–78888.
[50] Y.H. Hsu, A.T. Nguyen, Y.H. Chiu, J. Li, Y.J. Hsu, Appl. Catal. B: Environ. 185 (2016) 133–140.
[51] Z. Li, L. Ye, F. Lei, et al., Electrochim. Acta 188 (2016) 450–460.
[52] C. Zhai, M. Zhu, F. Pang, et al., ACS Appl. Mater. Interfaces 8 (2016) 5972–5980.
[53] F. Lei, Z. Li, L. Ye, Y. Wang, S. Lin, Int. J. Hydrogen Energ. 41 (2016) 255–264.
[54] S. Xu, L. Ye, Z. Li, Y. Wang, et al., Catalysts 6 (2016) 144.
[55] M.S. Zhu, C.Y. Zhai, M.J. Sun, Appl. Catal. B: Environ. 203 (2017) 108–115.
[56] J.Y. Hu, C.K. Yu, C.Y. Zhai, et al., Catal. Today 315 (2018) 36–45.
[57] C.Y. Zhai, M.J. Sun, M.S. Zhu, K. Zhang, Y.K. Du, Int. J. Hydrogen Energ. 42 (2017) 5006–5015.
[58] M.J. Sun, J.Y. Hu, C.Y. Zhai, M.S. Zhu, J.G. Pan, ACS Appl. Mater. Interfaces 9 (2017) 13223–13230.
[59] M.J. Sun, J.Y. Hu, C.Y. Zhai, M.S. Zhu, J.G. Pan, Electrochim. Acta 245 (2017) 863–871.
[60] C. Odetola, L.N. Trevani, E.B. Easton, Appl. Catal. B: Environ. 210 (2017) 263–275.
[61] J. Georgieva, S. Sotiropoulos, E. Valova, et al., J. Photochem. Photobiol. A-Chem. 346 (2017) 70–76.
[62] J. Zhang, N. Su, X. Hu, et al., RSC Adv. 7 (2017) 56194–56203.
[63] J. Zhang, X. Hu, F. Zhu, et al., Nanotechnology 28 (2017) 505603.
[64] J.Y. Hu, M.J. Sun, X.Y. Cai, et al., J. Taiwan Inst. Chem. E 80 (2017) 231–238.
[65] X. Hu, C. Ge, N. Su, et al., J. Alloys. Compd. 692 (2017) 848–854.
[66] J.Y. Hu, C.Y. Zhai, C.K. Yu, et al., J. Colloid Interface Sci. 524 (2018) 195–203.
[67] S. Hu, L. Jiang, Y. Tu, et al., J. Taiwan Inst. Chem. E 86 (2018) 113–119.
[68] C.Y. Zhai, M.J. Sun, L.X. Zeng, et al., Appl. Catal. B: Environ. 243 (2019) 283–293.
[69] X.D. Wang, M.J. Sun, Y. Guo, J.Y. Hu, M.S. Zhu, J. Colloid Interface Sci. 558 (2019) 38–46.
[70] H.F. Gao, C.Y. Zhai, N.Q. Fu, et al., J. Colloid Interface Sci. 561 (2020) 338–347.
[71] H.M. Zhang, J. He, C.Y. Zhai, M.S. Zhu, Chin. Chem. Lett. 30 (2019) 2338–2342.
[72] H.M. Zhang, C.Y. Zhai, P. Yang, et al., Energy Technol. 8 (2020) 1900731.
[73] Y. Wang, J.Y. Hu, C.Y. Zhai, et al., Energy Technol. 7 (2019) 1800539.
[74] S. Chang, A. Xie, S. Chen, J. Xiang, J. Electroanal. Chem. 719 (2014) 86–91.
[75] S. Kang, P. Shen, Electrochim. Acta 168 (2015) 104–110.
[76] A. Leelavathi, G. Madras, N. Ravishankar, J. Mater. Chem. A 3 (2015) 17459–17468.
[77] Z. Jin, Q. Wang, W. Zheng, X. Cui, ACS Appl. Mater. Interfaces 8 (2016) 5273–5279.
[78] A. Arabzadeh, A. Salimi, M. Ashrafi, S. Soltanian, P. Servati, Catal. Sci. Technol. 6 (2016) 3485–3496.
[79] H. Yang, L. He, Z. Wang, et al., ChemistrySelect 2 (2017) 9842–9846.
[80] M.J. Sun, C.Y. Zhai, J.Y. Hu, M.S. Zhu, J.G. Pan, J. Colloid Interface Sci. 511 (2018) 110–118.
[81] A.C. Queiroz, E.A. Ticianelli, J. Electrochem. Soc. 165 (2018) 123–131.
[82] C.Y. Zhai, J.Y. Hu, M.J. Sun, M.S. Zhu, Appl. Surf. Sci. 430 (2018) 578–584.

[83] J.Y. Hu, C.Y. Zhai, L.X. Zeng, Y.K. Du, M.S. Zhu, Catal. Sci. Technol. 8 (2018) 3562–3571.
[84] J.Y. Hu, C.Y. Zhai, H.F. Gao, et al., Sustain. Energ. Fuels 3 (2019) 439–449.
[85] H.F. Gao, C.Y. Zhai, H.M. Zhang, Energ. Technol. 7 (2019) 1900253.
[86] H.F. Gao, C.Y. Zhai, C. Yuan, Z. Liu, M.S. Zhu, Electrochim. Acta 330 (2020) 135214.
[87] S. Wasmus, A.J. Küver, J. Electroanal. Chem. 461 (1999) 14–31.
[88] X. Ren, P. Zelenay, S. Thomas, J. Davey, S. Gottesfeld, J. Power Sources 86 (2000) 111–116.
[89] S.C. Thomas, X.M. Ren, S. Gottesfeld, P. Zelenay, Electrochim. Acta 47 (2002) 3741–3748.
[90] R. Dillon, S. Srinivasan, A.S. Arico, V. Antonucci, J. Power Sources 127 (2004) 112–126.
[91] C. Yuan, H.F. Gao, Q.Y. Xu, et al., Appl. Surf. Sci. 521 (2020) 146431.
[92] H.F. Gao, C. Yuan, Z.L. He, et al., Energ. Technol. 8 (2020) 2000210.
[93] X.X. Li, K.L. Zhang, M. Zhou, et al., Sustain. Energ. Fuels 4 (2020) 2569–2582.
[94] E. Contreras, C. Palacios, B. Huerta, et al., ACS Appl. Mater. Interfaces 3 (2020) 8755–8764.
[95] Z.L. He, C. Yuan, H.F. Gao, et al., ACS Sustainable Chem. Eng. 8 (2020) 12331–12341.
[96] J. Willsau, J. Heitbaum, J. Electroanal. Chem. 194 (1985) 27–35.
[97] T. Iwasita, E. Pastor, Electrochim. Acta 39 (1994) 531–537.
[98] B. Bittins-Cattaneo, S. Wilhelm, E. Cattaneo, H.W. Buschmann, W. Vielstich, Phys. Chem. Chem. Phys. 92 (1988) 1210–1218.
[99] H. Hitmi, E. Belgsir, J.M. Léger, C. Lamy, R. Lezna, Electrochim. Acta 39 (1994) 407–415.
[100] J. Gootzen, W. Visscher, J. Van Veen, Langmuir 12 (1996) 5076–5082.
[101] V.M. Schmidt, R. Ianniello, E. Pastor, S. González, J. Phys. Chem. 100 (1996) 17901–17908.
[102] C.M. Miesse, W.S. Jung, K.J. Jeong, J. Power Sources 162 (2006) 532–540.
[103] Y. Zhu, S.Y. Ha, R.I. Masel, J. Power Sources 130 (2004) 8–14.
[104] C. Rice, S. Ha, R. Masel, P. Waszczuk, A. Wieckowski, J. Power Sources 111 (2002) 83–89.
[105] A. Serov, C. Kwak, Appl. Catal. B: Environ. 97 (2010) 1–12.
[106] L. An, R. Chen, J. Power Sources 329 (2016) 484–501.
[107] V. Livshits, E. Peled, J. Power Sources 161 (2006) 1187–1191.
[108] V. Livshits, A. Philosoph, E. Peled, J. Power Sources 178 (2008) 687–691.
[109] M.G. Hosseini, M.M. Momeni, J. Mol. Catal. A-Chem. 355 (2012) 216–222.
[110] M.G. Hosseini, M.M. Momeni, Appl. Cata. A: Gen 427 (2012) 35–42.
[111] T. Saida, N. Ogiwara, Y. Takasu, W. Sugimoto, J. Phys. Chem. C 114 (2010) 1390–13396.
[112] A. Pandikumar, S. Murugesan, R. Ramaraj, ACS Appl. Mater. Interfaces 2 (2010) 1912–1917.
[113] Z. Zhang, Y. Yuan, Y. Fang, et al., J. Electroanal. Chem. 610 (2007) 179–185.
[114] E. Hutter, J.H. Fendler, Adv. Mater. 16 (2004) 1685–1706.
[115] J.L. Wu, F.C. Chen, Y.S. Hsiao, et al., ACS Nano 5 (2011) 959–967.
[116] Z. Bian, T. Tachikawa, P. Zhang, M. Fujitsuka, T. Majima, J. Am. Chem. Soc. 136 (2014) 458–465.
[117] P.P. Fang, S. Chen, H. Deng, et al., ACS Nano 7 (2013) 9241–9248.
[118] N.S. Karan, A.M. Keller, S. Sampat, et al., Chem. Sci. 6 (2015) 2224–2236.
[119] S. Tripathi, M. Rani, N. Singh, Electrochim. Acta 167 (2015) 179–186.
[120] X. Zhang, Y. Liu, S.T. Lee, S. Yang, Z. Kang, Energy Environ. Sci. 7 (2014) 1409–1419.
[121] A. Sobhani, M.W. Knight, Y. Wang, et al., Nat. Commun. 4 (2013) 1–6.
[122] R. Long, K. Mao, M. Gong, et al., Angew. Chem. Int. Ed. 53 (2014) 3205–3209.
[123] M. Lu, C. Tsai, H. Chen, et al., Nano Energy 20 (2016) 264–271.
[124] Z. Zheng, T. Tachikawa, T. Majima, J. Am. Chem. Soc. 136 (2014) 6870–6873.
[125] H. Yang, L. He, Z. Wang, Electrochim. Acta 209 (2016) 591–598.
[126] H. Xu, P. Song, J. Wang, et al., ChemElectroChem 5 (2018) 1191–1196.
[127] H. Xu, P. Song, J. Wang, et al., ACS Sustain. Chem. Eng. 6 (2018) 7159–7167.
[128] Q. Wang, W. Zheng, H. Chen, et al., J. Power Sources 316 (2016) 29–36.
[129] S. Lee, Y. Wy, Y.W. Lee, K. Ham, S.W. Han, Small 13 (2017) 1701633.
[130] H. Xu, P.P. Song, C. Fernandez, et al., J. Taiwan Inst. Chem. E. 91 (2018) 316–322.
[131] H. Xu, P.P. Song, B. Yan, et al., ACS Sustain. Chem. Eng. 6 (2018) 4138–4146.
[132] G. Chen, M. Sun, J. Li, et al., Nanoscale 11 (2019) 18874–18880.
[133] S.P. Lim, A. Pandikumar, N.M. Huang, H.N. Lim, Int. J. Hydrogen Energ. 39 (2014) 14720–14729.
[134] J.A. Diaz-Real, E. Ortiz-Ortega, M.P. Gurrola, J. Ledesma-Garcia, L.G. Arriaga, Electrochim. Acta 206 (2016) 388–399.
[135] L. Wang, L. Xu, Y. Wang, Z.M. Su, R. Liu, Electrochim. Acta 155 (2015) 1–7.
[136] Q. Cai, W.T. Hong, C.Y. Jian, J. Li, W. Liu, ACS Sustain. Chem. Eng. 6 (2018) 4231–4238.